Available online at www.sciencedirect.com

ScienceDirect

Advances in Space Research 68 (2021) 2776–2790

ADVANCES IN SPACE RESEARCH (a COSPAR publication)

www.elsevier.com/locate/asr

An improved approach for testing gravitational redshift via satellite-based three frequency links combination

Ziyu Shen [a], Wen-Bin Shen [b,c,*], Tengxu Zhang [a], Lin He [a], Zhan Cai [a], Xiaojuan Tian [a], Pengfei Zhang [b]

[a] School of Resource, Environmental Science and Engineering, Hubei University of Science and Technology, Xianning 437100, China
[b] Time and Frequency Geodesy Research Center, Department of Geophysics, School of Geodesy and Geomatics, Wuhan University, Wuhan 430072, China
[c] Key Lab of Surveying Eng. and Remote Sensing, Wuhan University, Wuhan 430072, China

Received 20 January 2021; received in revised form 29 June 2021; accepted 5 July 2021
Available online 14 July 2021

Abstract

We propose a novel approach for testing the gravitational redshift based on frequency signals transmitted between a spacecraft and a ground station. The main idea is integrating one uplink signal from ground to spacecraft and two downlink signals from spacecraft to ground. Based on the integration and certain correction models, the gravitational shift of the signals between spacecraft and ground station can be detected at high precision level. The gravitational redshift effect can be used to validate the Einstein equivalence principle (EEP), which can be tested at about $10^{-6} \sim 10^{-8}$ levels in different cases for a short period (less than a month) if the stability of on-board atomic clock reach 10^{-17}/day. Compared to the scheme of Gravity Probe-A (GP-A) experiment conducted in 1976, in the new approach, any on-board signal transponders is not required, and the frequency values of the three links can be arbitrary. Since the hardware requirement is decreased, a number of spacecrafts can be candidates for a gravitational redshift experiment provided that they are able to emit two different frequency signals and receive a frequency signal from the ground.

Keywords: Relativity; Gravitational redshift; Gravitational potential; Frequency link

1. Introduction

The gravitational redshift was predicted by general theory of relativity (Einstein, 1915) as a characteristic of Einstein equivalence principle (EEP). Supposing two clocks located at various positions, the EEP predicts $\Delta v/v = \Delta U/c^2$ for stationary clocks, where $\Delta v/v$ and ΔU are the fractional frequency difference and gravitational potential difference between the two clocks respectively. Since the gravitational potential is a very fundamental quantity in geoscience associated with the orthometric height, the EEP has great potential in geodesy applications. Although Bjerhammar (1985) presented the method of measuring gravitational potential difference by clocks transportation more than 35 years ago, it was not until the last few years that this method (denotes as relativistic approach) was considered. The reason is that required high-precision atomic clocks were not available until recent years. However, by reaching 10^{-18} level (Oelker et al., 2019; Nakamura et al., 2020) for the relative stability of optical atomic clocks, the theoretical precision of potential determination can reach 0.1 m^2s^{-2} level (equivalent to 1 cm in height). Recently, various kinds of methods appear to

* Corresponding author at: Time and Frequency Geodesy Research Center, Department of Geophysics, School of Geodesy and Geomatics, Wuhan University, Wuhan 430072, China.
E-mail addresses: wbshen@sgg.whu.edu.cn (W.-B. Shen), txzhangsgg@whu.edu.cn (T. Zhang), caiz@hbust.edu.cn (Z. Cai), pfzhang@whu.edu.cn (P. Zhang).

https://doi.org/10.1016/j.asr.2021.07.004
0273-1177/

determine the geopotential based on time and frequency signals transfer, such as by direct clock transportation (Kopeikin et al., 2016; Grotti et al., 2018), based on frequency signals transmitted in optical fiber (Takano et al., 2016; Lion et al., 2017; Shen et al., 2019), and based on frequency signals transmitted in free space (Shen et al., 2016; Shen et al., 2017).

To apply the general theory of relativity into gravitational potential determination, it is generally assumed that the EEP is correct, which is not necessarily the truth. Indeed, general relativity is incompatible with quantum theory implying an additional parameter α in the basic gravitational redshift equation (Will, 2014):

$$z = \frac{\Delta f_{grav}}{f} = (1+\alpha)\frac{\Delta U}{c^2}, \tag{1}$$

where $\alpha = 0$ is based on the general relativity, while in unified theories α is normally a small non-zero amount. Therefore, the gravitational redshift tests are the key research field in theoretical physics. Since the first experimental verification of gravitational redshift performed by Pound and Rebka (1960), a growing number of redshift tests have been conducted. Most of the tests are performed on ground, however, a test between a spacecraft and a ground station has more advantages because of a much larger ΔU. A few spacecraft-based experiments for gravitational redshift have been conducted until now. The Gravity Probe A (GP-A) mission is the most famous test carried out in 1976 (Vessot and Levine, 1979; Vessot et al., 1980). It validated that $|\alpha| \leqslant 7 \times 10^{-5}$. The GP-A mission was the most accurate test of the gravitational redshift for a long time until 2018. It was when two research teams published papers almost simultaneously with precision of $(0.19 \pm 2.48) \times 10^{-5}$ (Delva et al., 2018) and $(4.5 \pm 3.1) \times 10^{-5}$ (Herrmann et al., 2018) based on experiments performed with the two Galileo satellites (GSAT0201 and GSAT0202) in failed, highly eccentric orbits, ideally suited for the EEP tests. The most accurate gravitational redshift test on ground was reported by Takamoto et al. (2020) achieving the precision level of $\alpha = (1.4 \pm 9.1) \times 10^{-5}$. There will be also a few planned spacecraft experiments in the near future. For instance, the Atomic Clock Ensemble in Space (ACES) mission aims to test gravitational redshift at a level of 10^{-6} (Cacciapuoti and Salomon, 2011; Meynadier et al., 2018), the Space–Time Explorer and QUantum Equivalence Space Test (STE-QUEST) aim to test gravitational redshift at a level of 10^{-7} (Altschul et al., 2015), although STE-QUEST has been abandoned in favor of other missions recently (Wikipedia contributors, 2021).

In the GP-A mission, a very useful scheme was adopted (Kleppner et al., 1970; Vessot and Levine, 1979). It combines a go-return link from ground to satellite to ground and a one-way link from satellite to ground (It means that there are three microwave links in total: one uplink from ground to satellite and two downlinks from satellite to ground) to cancel out the nonrelativistic Doppler, ionospheric and tropospheric effects. However, the subsequent spacecraft experiments did not adopt the same scheme. The main reason is that the GP-A scheme requires a phase-coherent transponder on-board to transmit the uplink signal back to the ground. Moreover, the signals' frequency values of the three links must satisfy definite conditions for the ionospheric shift cancellation (Vessot and Levine, 1979). These prerequisites are hardly satisfied by a spacecraft not specializing in gravitational redshift test such as the GP-A. For instance, the Galileo satellites are part of a global navigation satellite system (GNSS), for which the gravitational redshift experiments are based on a single one-way link (Delva et al., 2015). The RadioAstron satellite was used in another recently conducted gravitational redshift experiment (Litvinov et al., 2018; Nunes et al., 2020), which mainly focuses on Very Long Baseline Interferometer (VLBI) measurements (Kovalev et al., 2014). Although the satellite is equipped with a phase-coherent transponder, it cannot simultaneously emit two different frequency signals to ground, and the frequency combination cannot cancel completely out the ionospheric shift. With a scheme similar to GP-A (but not as good as), the RadioAstron experiment's precision is also limited to the 10^{-5} level (Litvinov et al., 2018). No published details exist on the method of gravitational redshift tests planned in STE-QUEST and ACES, however, it seems that the GP-A scheme is not applicable due to no transponder equipped on-board.

To date, the gravitational redshift tests are still limited to $10^{-5} \sim 10^{-6}$ level without obvious enhancements compared to the GP-A mission conducted over 40 years ago. The GP-A scheme is obviously superior for errors elimination. To take advantages of the GP-A's frequency combination while reducing the hardware prerequisites, we proposed a novel technique to examine the gravitational redshift regarded as an enhanced version of GP-A method. Three space links are also required by the novel method including a uplink from ground to satellite and two downlinks from satellite to ground. However, the two downlinks can be independent of the uplink, which means that no on-board transponder is required. Moreover, the signals' frequency values of the three links can be arbitrary, hence most of the microwave frequency signals adopted by a spacecraft (e.g. GNSS, space station, communication satellite, et al.) are suitable for the gravitational shift test. However, the precision of gravitational redshift test based on our proposed method will be better than the results of GP-A experiment, because more detailed error correction models are adopted, and the stability of atomic clocks currently (or in the near future) available are better than that of the GP-A on-board clock. By reducing the hardware requirements, many spacecrafts can perform a high precision gravitational redshift test experiment, such as the planned ACES on board the International Space Station (ISS) and similar experiments on China Space Station

(CSS). They both have at least one uplink and two downlinks (Meynadier et al., 2018). Furthermore, since at least two microwave downlinks are included in a modern GNSS satellite, it can also perform a similar gravitational potential test once by arming with a frequency signal's receiver for an uplink.

This paper is organized as follows. In Section 2 we provide our three frequencies combination approach to examine the gravitational redshift with a spacecraft. The principle of errors cancellation is also represented. In Section 3 we analyze the influences of various error sources in detail and provide some correction models for certain main error sources. Moreover, the theoretical precision of the determined α is consequently presented. The conclusion is provided in Section 4 along with discussing the potential of our approach for EEP validation and gravitational potential determination experiments. Furthermore, some possible improvements are presented as the future work.

2. Method

2.1. Frequency shift of a one-way signal link

Considering a one-way frequency signal link from a spacecraft to a ground station (or reverse direction), the frequency shift $\Delta f = f_r - f_s$ between the received frequency f_r at receiver and the emitted frequency f_s at sender can be stated as:

$$\Delta f = \Delta f_{dop} + \Delta f_{rel} + \Delta f_{ion} + \Delta f_{trop} + \Delta f_{oth} \tag{2}$$

where Δf_{dop} is the classical Doppler shift, Δf_{rel} is the frequency shift caused by relativistic effects including transverse Doppler shift, gravitational redshift, and Shapiro effect, Δf_{ion} and Δf_{trop} denote ionospheric and tropospheric shift, respectively, Δf_{oth} represents various other minor effects resultant from for instance phase center motion, magnetic field, and instrumental (including observation noise). Since in practice Δf is normally the observed value, we will briefly analyze the right-hand side terms of Eq. (2) to discover the Δf_{rel} component. Consequently, the gravitational redshift Δf_{grav} value is obtained out of the Δf_{rel} component.

For convenience, the Geocentric Inertial Coordinate System is adopted in this work. The classical Doppler shift Δf_{dop} is stated as:

$$\Delta f_{dop} = -f_s \frac{\dot{R}_{sr}}{c}, \tag{3}$$

where c represents the speed of light in vacuum, $\boldsymbol{R_{sr}}$ denotes the position vector between receiver and sender, $R_{sr} = |\boldsymbol{R_{sr}}|, \dot{R}_{sr} = \mathrm{d}R_{sr}/\mathrm{d}t$ is the radial velocity of the spacecraft relative to the ground station. If the required precision of α is 10^{-6}, the precision of $\dot{R}_{sr}$ should be better than 10^{-8} m/s, which is far beyond the current range rate precision level $10^{-5} \sim 10^{-6}$ m/s for GNSS satellite. Thus, some techniques must be run to cancel the classical Doppler shift, (Section 2.2).

The relativistic frequency shift Δf_{rel} is rather complicated for derivation since it is related to the general theory of relativity. Various scholars have made efforts to formulate the expression of Δf_{rel} at different precision level (Vessot and Levine, 1979; Blanchet et al., 2001; Linet and Teyssandier, 2002; Shen et al., 2017). Here, we adopted the expressions presented by Blanchet et al. (2001) including the c^{-3} terms and satisfying the precision requirement to the order of 10^{-17} in fractional frequency:

$$\begin{aligned}\frac{\Delta f_{rel}}{f_s} = & \frac{\left(U_r+0.5v_r^2\right)-\left(U_s+0.5v_s^2\right)}{c^2} \\ & + \frac{\boldsymbol{N_{sr}}\cdot\boldsymbol{v_r}\left(U_s+0.5v_s^2\right)-\boldsymbol{N_{sr}}\cdot\boldsymbol{v_s}\left(U_r+0.5v_r^2\right)+q_r-q_s}{c^3} + O(c^{-4}),\end{aligned} \tag{4}$$

where U_s and U_r represent the gravitational potentials of emitter and receiver, respectively. $\boldsymbol{v_s}$ and $\boldsymbol{v_r}$ denote velocity vector of emitter and receiver respectively, $v_s = |\boldsymbol{v_s}|, v_r = |\boldsymbol{v_r}|, \boldsymbol{N_{sr}} = \boldsymbol{R_{sr}}/R_{sr}, O(c^{-4})$ are omitted terms of c^{-4} and higher, q_s and q_r denote Shapiro effect as (Blanchet et al., 2001):

$$\begin{aligned} q_s &= 4GM\frac{(r_s+r_r)\boldsymbol{N_{sr}}\cdot\boldsymbol{v_s}+R_{sr}\boldsymbol{n_s}\cdot\boldsymbol{v_s}}{R_{sr}^2-(r_s+r_r)^2} + O(J_2), \\ q_r &= 4GM\frac{(r_s+r_r)\boldsymbol{N_{sr}}\cdot\boldsymbol{v_r}+R_{sr}\boldsymbol{n_r}\cdot\boldsymbol{v_r}}{R_{sr}^2-(r_s+r_r)^2} + O(J_2),\end{aligned} \tag{5}$$

where $GM = 3.986004418 \times 10^{14}$ m^3/s^2 is the geocentric gravitational constant of Earth, $\boldsymbol{r_s}$ and $\boldsymbol{r_r}$ are position vectors of emitter and receiver respectively, $r_s = |\boldsymbol{r_s}|, r_r = |\boldsymbol{r_r}|, \boldsymbol{n_s} = \boldsymbol{r_s}/r_s, \boldsymbol{n_r} = \boldsymbol{r_r}/r_r, O(J_2)$ are the omitted terms caused by the J_2-term of the Earth. It is worth noting that the Eqs. (4) and (5) presented here are slightly different from Blanchet et al. (2001). The reason is that the classical Doppler effect is not included in Δf_{rel} here in contrary to the original equations in Blanchet et al. (2001).

Since the $(U_r - U_s)/c^2$ component is included in Eq. (4) associated with gravitational redshift Δf_{grav}, it can be directly adopted to examine the EEP once the relativistic effect Δf_{rel} is determined (the position, gravitational potential, and velocities of the two points in the right-hand side of Eq. (4) are known values for an EEP test). The errors represented by the omitted terms and the uncertainties of the certain values in the right-hand side of Eq. (4) are discussed in Section 3.1.

For the ionospheric shift Δf_{ion}, we have the following expression (Namazov et al., 1975):

$$\Delta f_{ion} = -\frac{f_s}{c}\frac{\mathrm{d}}{\mathrm{d}t}\int_L (n_i - 1)\mathrm{d}s, \tag{6}$$

where n_i denotes the phase index of refraction of ionosphere, and L represents the path of the signal's propagation. The refractive index n_i can be expressed as (Davies et al., 1962):

$$n_i = 1 - 40.3\frac{N_e}{f_s^2} + O\left(f^{-3}\right), \tag{7}$$

where N_e is electron density per m^3 (cubic m), the terms higher than f^{-3} are omitted since they are at least two magnitudes smaller than the f^{-2} term for microwave frequencies (> 1 GHz) (Hoque and Jakowski, 2007). They will be discussed in detail in Section 3.2. Substituting Eq. (7) into Eq. (6), we have:

$$\Delta f_{ion} = \frac{40.3}{cf_s}\frac{\mathrm{d}}{\mathrm{d}t}TEC, \tag{8}$$

where $TEC = \int_L N_e \mathrm{d}s$ denotes total electron content representing the total number of free electron along a 1 m^2 column of the signal's path.

The tropospheric shift Δf_{trop} is stated as:

$$\Delta f_{trop} = -\frac{f_s}{c}\frac{\mathrm{d}}{\mathrm{d}t}\int_L (n_t - 1)\mathrm{d}s, \tag{9}$$

where n_t is the refractive index of troposphere, which is normally estimated formulas follows (Rüeger, 2002):

$$n_t = 1 + \left(k_1\frac{p_d}{T} + k_2\frac{p_w}{T} + k_3\frac{p_w}{T^2}\right)\times 10^{-6} + \epsilon, \tag{10}$$

where T represents temperature in Kelvin (K), p_d and p_w denote the partial pressures (hPa) of dry air and of water vapor, respectively, k_1, k_2 and k_3 are constant parameters, and ϵ is uncertainty. A recent estimation presents $k_1 = 77.6890, k_2 = 71.2952$ and $k_3 = 375463$ (Rüeger, 2002; Corstanje et al., 2017), and the uncertainty ϵ is less than 0.1% of the second term ($< 3\times 10^{-7}$ for standard atmosphere), which can be omitted in our study. We represent the second term of Eq. (10) as N for convenience, therefore, the tropospheric shift Δf_{trop} is:

$$\Delta f_{trop} = -\frac{f_s}{c}\frac{\mathrm{d}}{\mathrm{d}t}\int_L N\mathrm{d}s. \tag{11}$$

Although by Eq. (11), a method is provided to estimate Δf_{trop}, the pressures and temperatures along the signal's paths are required for calculation that are difficult to precisely determine. However, the tropospheric shift Δf_{trop} is proportional to frequency f_s (same as the classical Doppler shift Δf_{dop}). Thus, we will manage to cancel it via the frequency combination technique explained in the following subsection.

If we do not consider the clock errors, the ultimate term Δf_{oth} in Eq. (2) only determines a small value of frequency shift which can be basically omitted for the 10^{-17} precision requirement. Nevertheless, the clock errors might greatly affect the precision of the EEP test experiment at some cases. This will be discussed in section Section 3.4.

2.2. Frequency shift of three links combination

A combination of one uplink and two downlinks are adopted in the GP-A experiment. One of the downlinks is a transmission of the uplink by a transponder. This setup requires a transponder increasing the burden of payload, and results in a time delay during the transmitting procedure. A special frequency combination of the three links was also adopted by the GP-A experiment to cancel out the ionospheric shift. This makes a normal spacecraft unsuitable for similar experiments if it is not special designed for gravitational shift test. To overcome these drawbacks, we presented a new kind of combination (as depicted in Fig. 1) not requiring a signal transponder. Moreover, arbitrary microwave frequency values can be adopted (1 ∼ 40 GHz From a practical point of view).

The setup of the frequency combination (Fig. 1) is briefly described as follows. The signals are exchanged between a ground station P and a spacecraft S. A signal of frequency f_0 is emitted by the ground station P emits at time t_0; the signal is then received by spacecraft S as frequency f_0' at time t_1. Two signals of frequency f_1 and f_2 are also emitted by the spacecraft S at time t_1. These signals are then received by ground station as frequency f_1' and f_2' at time t_2, while the position of ground station is changed to P' due to Earth's rotation. The frequency values of f_0, f_1 and f_2 are unlimited as long as they are in microwave band (but f_1 should not be equal with f_2, otherwise the two downlink signals cannot be distinguished). We represent the frequency shifts of the three links as $\Delta f_0 = f_0' - f_0, \Delta f_1 = f_1' - f_1, \Delta f_2 = f_2' - f_2$, and set f_0 as reference frequency presenting $f_1 = af_0, f_2 = bf_0$ (a and b are known scaling factors). Thus, we take the following combination of frequency shifts as an output value f_{out}:

$$\begin{aligned} f_{out} &= b^{-1}\cdot\Delta f_2 - \tfrac{\Delta f_0 + a^{-1}\cdot\Delta f_1}{2} \\ &= b^{-1}\cdot f_2' - 0.5a^{-1}\cdot f_1' - 0.5f_0'. \end{aligned} \tag{12}$$

Since f_{out} can be acquired by a combination of the observations f_0', f_1' and f_2' from Eq. (12), it can also be considered as an observation value. In Eq. (12) the tropospheric shift and classical Doppler shift are almost cancelled out (the remained residuals are resultant from the position difference of P and P', which will be analyzed in Section 3.3). The ionospheric shift and other small influencing factors still remain. To further analyze the frequency combination f_{out}, the one-way frequency shift Eq. (2) is rewritten as follows:

$$\Delta f_i = f_i\cdot C_{dop} + \Delta f_{rel(i)} + f_i^{-1}\cdot C_{ion} + f_i\cdot C_{trop} + \Delta f_{oth(i)}, \quad (i = 0, 1, 2) \tag{13}$$

where $i = 0, 1, 2$ indicates three different links, C_{dop}, C_{ion} and C_{trop} are counterparts (with no relations to i, i.e. they are independent of frequency) of classical Doppler shift, ionospheric shift and tropospheric shift. Their frequency factors f_i are extracted based on Eqs. (3), (8) and (11) respectively. Although relativistic effects Δf_{rel} also contain factor f_i as shown in Eq. (4), its counterpart has relation to i. Therefore, Δf_{rel} is remained unchanged in Eq. (13) since it cannot be cancelled out by the three link combination. f_{oth} is the sum of all other minor effects, much of which

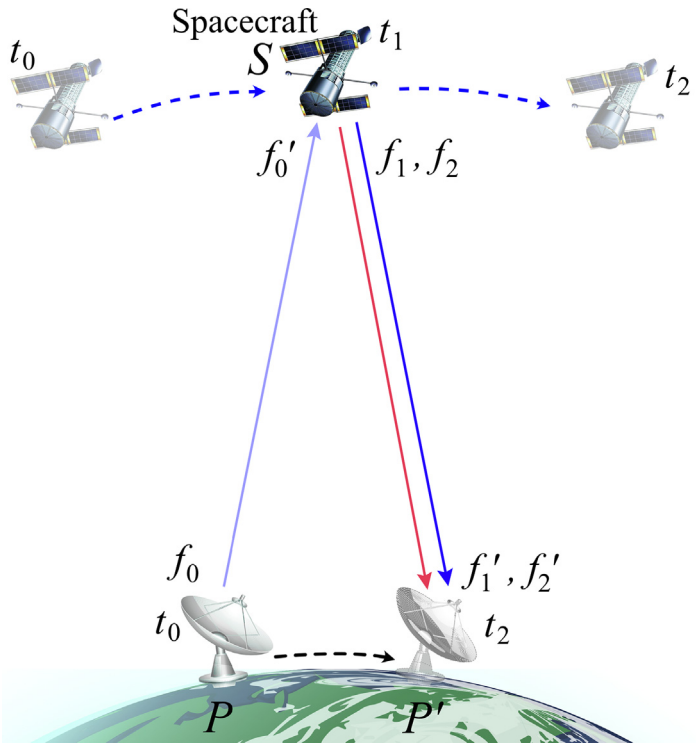

Fig. 1. The combination of three frequency links. Ground station P emits a frequency signal f_0 at time t_0. The signal is received by spacecraft S as f_0' at time t_1. Spacecraft S also emits two frequency signals f_1 and f_2 at time t_1. Furthermore, the ground station receives the two signals as f_1' and f_2' at time t_2, when its position is changed to P' due to the Earth's rotation. The frequency values of f_0, f_1' and f_2' are measured according to the clock of ground station P; the frequencies of f_0', f_1 and f_2 are measured according to the on-board clock of spacecraft. These frequency values will be integrated according to Eq. (12).

do not have the factor f_i, hence we leave it unchanged as well.

It is worth noting that the relativistic effects of uplink $\Delta f_{rel(0)}/f_0$ are opposite to that of downlinks $\Delta f_{rel(1)}/f_1$ and $\Delta f_{rel(2)}/f_2$. Thus, we set $\Delta f_{rel}/f_0 = \Delta f_{rel(2)}/f_2 = \Delta f_{rel(1)}/f_1 = -\Delta f_{rel(0)}/f_0$ for convenience, and the observations f_{out} can be stated as:

$$f_{out} = C_1 \cdot \Delta f_{rel} + C_2 \cdot \frac{40.3\dot{TEC}}{c \cdot f_0} + C_3, \tag{14}$$

where $\dot{TEC}$ is the change rate $\mathrm{d}TEC/\mathrm{d}t$, the coefficients C_1, C_2 and C_3 are determined as:

$$C_1 = b^{-1} - 0.5a^{-1} + 0.5 \tag{15}$$

$$C_2 = b^{-2} - 0.5a^{-2} - 0.5 \tag{16}$$

$$C_3 = b^{-1} \cdot \Delta f_{oth(2)} - 0.5a^{-1} \cdot \Delta f_{oth(1)} - 0.5\Delta f_{oth(0)}, \tag{17}$$

where the tropospheric shift and classical Doppler shift are cancelled out. Although these cancellations are not completely performed due to non-identical signal's path of uplink and downlinks in a real case, here, they are ignored and the residuals will be analyzed and corrected in Section 3.3

By ignoring the small value C_3 in Eq. (14), Δf_{rel} can be deduced from Eqs. (14)–(17) once the value $\dot{TEC}$ is determined. A special case is $C_2 = 0$, viz. $b^{-2} - 0.5a^{-2} - 0.5 = 0$, thus, the ionospheric shift will also be cancelled out (similar method is a prerequisite in GP-A experiment). However, this cancellation needs a dedicated selection of three frequencies f_0, f_1 and f_2 that is hardly satisfied by most of the spacecrafts. There are no limitations in our technique for selecting the three frequencies, hence, we only consider the cases when $C_2 \neq 0$. Since two frequency downlinks exist, we can solve the TEC value by measuring the time delay between the two signals (Brunner and Gu, 1991; Hernández-Pajares et al., 1999). This technique has been extensively used in GNSS ranging as ionosphere-free observations. It will be briefly explained in the following subsection.

2.3. The determination of TEC

The time delay of a microwave frequency signal is relevant to its group index of refraction n_g (different from phase index of refraction n_i described in Section 2.1). It can be stated as (Leick et al., 2015):

$$n_g = 1 + 40.3\frac{N_e}{f^2} + O(f^{-3}), \tag{18}$$

where f is the signal's frequency, and higher order terms than f^{-2} are omitted. Then, we have the well-known

expression to estimate the impact of ionosphere I_{ion}, indeed, a time delay expressed in distance:

$$I_{ion} = \int \left(n_g(s) - 1\right) \mathrm{d}s = \frac{40.3}{f^2} TEC, \tag{19}$$

where the integration occurs over the propagation path of the signal, with $n_g(s)$ representing the index of refraction at various places s.

Returning to our three links combination explained in Section 2.2, the propagation paths of the two downlink signals f_1 and f_2 are identical since they are emitted at the same time (the insignificant difference resultant from velocity difference is negligible), consequently, their TEC are also identical. Suppose that for a certain time t, the time interval between signal's emitting event and receiving event for frequencies f_1 and f_2 are t_1 and t_2 respectively, then, we have:

$$\begin{aligned} s(t) &= c \cdot t_1(t) - \tfrac{40.3TEC(t)}{f_1^2} - I_{other(1)}(t) \\ s(t) &= c \cdot t_2(t) - \tfrac{40.3TEC(t)}{f_2^2} - I_{other(2)}(t), \end{aligned} \tag{20}$$

where s is the distance between the ground station and the spacecraft, c is the speed of light in vacuum, $I_{other(1)}$ and $I_{other(2)}$ are impact of other sources (such as clock errors, troposphere, and instrumental delay) while neglecting higher order ionospheric terms for the two signals respectively. Since I_{other} has no relations to the signal's frequency (only the ionosphere acts as a dispersive medium at microwave frequency), we have $I_{other(1)} = I_{other(2)}$, and the $TEC(t)$ can be solved by Eq. (20):

$$TEC(t) = \frac{c \cdot \Delta t(t) \cdot f_1^2 \cdot f_2^2}{40.3\left(f_2^2 - f_1^2\right)}, \tag{21}$$

where $\Delta t(t) = t_2(t) - t_1(t)$ can be considered as the time difference between the signal f_1 and f_2 received by ground station at time t, for signals emitted at the same time. Based on Eq. (21), to obtain the value of $TEC(t)$, the time difference $\Delta t(t)$ needs to be recorded. The former effects can be well modeled and estimated by modulating some marking signal into f_1 and f_2. Continuously measuring $TEC(t)$, its time derivative $\dot{TEC}(t)$ can also be estimated:

$$\dot{TEC}(t) = \frac{TEC(t+\tau) - TEC(t)}{\tau} \tag{22}$$

where $t + \tau$ is the next measurement time followed by t.

2.4. Validation of the Einstein equivalence principle

If the EEP is valid, then, value according to Eq. (4), the predicted Δf_{rel} should satisfy Eq. (14) as:

$$\left| \Delta f_{rel} + \frac{C_2}{C_1} \cdot \frac{40.3\dot{TEC}}{c \cdot f_0} + \frac{C_3}{C_1} - \frac{1}{C_1} f_{out} \right| < \delta f_{all} \tag{23}$$

where δf_{all} is the summation of all errors for the left side terms, which will be analyzed in detail in Section 3. The δf_{all} also reflects the precision of EEP test experiment. Based on the gravitational redshift testing formula Eq. (1), the uncertainty of parameter α is obtained as

$$\delta\alpha = \frac{\delta f_{all}/f_0}{\Delta U/c^2}, \tag{24}$$

where $\delta\alpha$ denotes the precision achieved for validating the EEP by our three links combination technique. In the next section, we will analyze the error magnitudes of various error sources, develop error correction models for certain error sources, and ultimately estimate the numerical values of $\delta\alpha$ based on various conditions.

3. Error analyses and correction models

In this section, we will analyze the influence of the higher order terms or error terms omitted in previous calculation, of the last term C_3 in Eq. (14), and of the path discrepancy between uplink and downlink. Some correction models are also established based on the error estimations. It is worth noting that the effects of path discrepancy are separately analyzed in Section 3.3, therefore, other error effects are analyzed under the assumption that the path of downlink and uplink are identical.

3.1. Relativistic effects

The errors of relativistic effects in Eqs. (4) and (5) for one-way signal link are first originated from the omitted high order terms. Previous studies indicate that the terms of $O(c^{-4})$ in Eq. (4) account for a few parts in 10^{-19} or less in the vicinity of the Earth (Wolf and Petit, 1995; Delva et al., 2019), which is neglectable. Suppose the elevation angle of spacecraft is restricted to the higher than 20°, then, the amount of Shapiro effect correction $(q_r - q_s)/c^3$ in Eqs. (4) is about 7.2×10^{-16} for GNSS satellite and about 1.5×10^{-15} for ISS at most. Since the effect of J_2-term for gravitational field outside the Earth is less than 1/300 of the main term, the uncertainty of Shapiro correction will not exceed 2.4×10^{-18} and 5.0×10^{-17} for GNSS satellite and ISS, respectively. When higher accuracy is needed, the gravity filed of Earth including the J_2-term needs to be adopted, which is not necessary in this work.

Other important error sources in Δf_{rel} are the uncertainties of gravitational potentials, velocities and positions of the two points. The gravitational potential field is time-varying around the world, and it is normally divided into the static part U^{static} and the temporary part U^{temp}, as:

$$U = U^{static} + U^{temp}. \tag{25}$$

The temporary part U^{temp} is mainly originated from the Earth tides, external masses (Sun and Moon) and irregular displacements of Earth's surface. The former two effects can be well modeled and estimated by an Earth tide model (e.g. Tsoft, see Van Camp and Vauterin, 2005) and planetary and lunar ephemerides (JPL, Folkner et al., 2014). However, the irregular displacements (e.g. ice melting, sea level

rise, snow fall, etc.) are normally insignificant and negligible for a short period of observations (several days to a month for our test). If long-term observation is required, these effect can also be corrected based on various mass migration models if necessary. At most cases, the residual errors of U^{temp} will not exceed 1 cm (associated with the location of ground station), since most of the components of U^{temp} are periodical and can be corrected. The static part U^{static} can be determined via an Earth gravity model (e.g. EGM2008 Pavlis et al., 2012) integrated with geometric leveling. Specifically, the gravitational potential at spacecraft can be determined by gravity model (about 1 cm in precision at the GNSS satellite orbit), however, the gravitational potential at ground station is determined by leveling and gravimeter with a precision better than 1 cm (Sánchez and Sideris, 2017). Thus, it is concluded that the uncertainty is $\delta U \sim 0.1\ \mathrm{m^2 s^{-2}}$ for both the ground and the spacecraft.

The velocity and position accuracy for a spacecraft is about 1 cm in position and 10^{-5} m/s in velocity (Kang et al., 2006; Griffiths and Ray, 2009; Wang et al., 2020). The position accuracy for a static ground station is better than 1 cm; the velocity uncertainty is negligible since it is much smaller than that of the spacecraft. Thus, for the one-way case explained by Eq. (4), we have $\delta U_s = \delta U_r \sim 0.1\ \mathrm{m^2 s^{-2}}$, $\delta v_s \sim 10^{-5}$ m/s, $\delta r_s = \delta R_{sr} \sim 10^{-2}$ m, $\delta r_r \sim 10^{-2}$ m. Then, considering the uncertainty of Shapiro correction, the uncertainty of Δf_{rel} (represented as δf_{rel}) can be estimated through the law of error propagation based on Eq. (4). Numerical calculations indicate $\delta f_{rel}/f_0 \sim 2.9 \times 10^{-18}$ for the GNSS satellite case, $\delta f_{rel}/f_0 \sim 5.0 \times 10^{-17}$ for the ISS case.

3.2. Ionospheric shift

The effect of ionospheric shift is originated from the terms $O(f^{-3})$ in Eqs. (7) and (18). The precise formulae expressing n_i and n_g read (Petrie et al., 2011):

$$n_i = 1 - \frac{40.3N_e}{f^2} - \frac{40.3N_e A_g B|\cos\theta|}{f^3} - \frac{(40.3N_e)^2}{2f^4} + O(f^{-5}), \tag{26}$$

$$n_g = 1 + \frac{40.3N_e}{f^2} + \frac{80.6N_e A_g B|\cos\theta|}{f^3} + \frac{3(40.3N_e)^2}{2f^4} + O(f^{-5}), \tag{27}$$

where $A_g = 2.80 \times 10^{10}$ sA/kg denotes constant coefficient, B represents the modulus of geomagnetic filed vector $\boldsymbol{B}$, and θ is the angle of between signal propagation direction and vector $\boldsymbol{B}$. $O(f^{-5})$ are high order terms and safely neglected. It is obvious that the effect of ionosphere will rapidly decrease by increasing signal's frequency f. Suppose that f is about 1.4 GHz (the case of GPS carrier frequency), then if $TEC = 6 \times 10^{17}\ \mathrm{el{\cdot}m^{-2}}$ and $B = 5 \times 10^{-5}$ Tesla (they are normally smaller in real cases), the maximum influence of f^{-3} and f^{-4} terms for Eq. (20) are about 1 cm and 1 mm, respectively (Hoque and Jakowski, 2007; Leick et al., 2015). Corresponding to $\delta TEC \sim 10^{14}\ \mathrm{el{\cdot}m^{-2}}$, the clock uncertainty will also increase δTEC. However, in this subsection, we just neglected the clock error which will be deliberated in Section 3.4 separately). Suppose the relative precision of $\dot{TEC}$ is the same as that of TEC, then since a typical $\dot{TEC}$ is normally smaller than $10^{15}\ \mathrm{el{\cdot}m^{-2}{\cdot}s^{-1}}$ (Pi et al., 1997), $\delta\dot{TEC}$ is estimated as $< 2 \times 10^{11}\ \mathrm{el{\cdot}m^{-2}{\cdot}s^{-1}}$.

Similarly, we can estimate the effect of $O(f^{-3})$ term in Eq. (7). Then, combined with $\delta\dot{TEC}$, the uncertainty δf_{ion} for Eq. (8) is about 1.1×10^{-4}. Obviously, this accuracy is insufficient for a high precision EEP test, hence the high order terms of ionospheric refractive index n_i and n_g must be considered.

There are two approaches to enhance the accuracy of Δf_{ion}. The first approach is to increase the signal's frequency. For instance, if the frequency f in Eqs. (26) and (27) increase by a factor of 2.2 times, $\delta f_{ion}/f$ will decrease one order of magnitude. Moreover, a 3.7 -fold increment of f will result in two orders of magnitude decrease in $\delta f_{ion}/f$. Regarding ACES where the frequencies reach $13 \sim 15$ GHz (Savalle et al., 2019), the relative uncertainty $\delta f_{ion}/f$ is about 10^{-16}, equal to about 1 m in potential difference. Nevertheless, the error magnitude will be magnified since one of the downlink frequencies of ACES is only 2.248 GHz resulting in a large C_2 value in Eq. (14). Detailed numerical estimations of GPS and ACES cases are provided in Section 3.5, a moderate increase of this downlink frequency of ACES to lower the C_2 value will help improve the precision.

The second approach is to consider the f^{-3} and f^{-4} terms in Eqs. (26) and (27). We can adopt an Earth's magnetic field model (the International Geomagnetic Reference Field (IGRF) for instance, Thébault et al. (2015)) to calculate the influence of the high order terms and estimate the magnetic value B and. To avoid the cumbersome calculation of the magneto-ionic interaction (between the geomagnetic field and the ionosphere) along ray paths, we assume the ionosphere as a thin layer at a certain altitude and calculate the magnetic field vector $\boldsymbol{B}$ at the ionospheric pierce point (IPP), as depicted in Fig. 2. Our estimation is also simplified by the thin layer assumption for the f^{-4} term since we have $\int_L N_e^2 \mathrm{d}s \approx TEC^2$. Accordingly, the expression for ionospheric shift Δf_{ion} is expanded as:

$$\begin{aligned}\Delta f_{ion} = {} & \frac{40.3}{cf_s}\frac{\mathrm{d}}{\mathrm{d}t}TEC(t) \\ & + \frac{1.128 \times 10^{12} B(t)\cos\theta \cdot TEC(t)}{cf_s^3} \\ & + \frac{812 TEC(t)^2}{cf_s^4},\end{aligned} \tag{28}$$

and the equations for solving TEC are expanded as:

$$\begin{aligned} s(t) &= c \cdot t_1(t) - \tfrac{40.3TEC(t)}{f_1^2} - \tfrac{2.256\times10^{12}B(t)\cos\theta\cdot TEC(t)}{f_1^3} - \tfrac{2437TEC(t)^2}{f_1^4} - I_{other(1)}(t) \\ s(t) &= c \cdot t_2(t) - \tfrac{40.3TEC(t)}{f_2^2} - \tfrac{2.256\times10^{12}B(t)\cos\theta\cdot TEC(t)}{f_2^3} - \tfrac{2437TEC(t)^2}{f_2^4} - I_{other(2)}(t), \end{aligned} \tag{29}$$

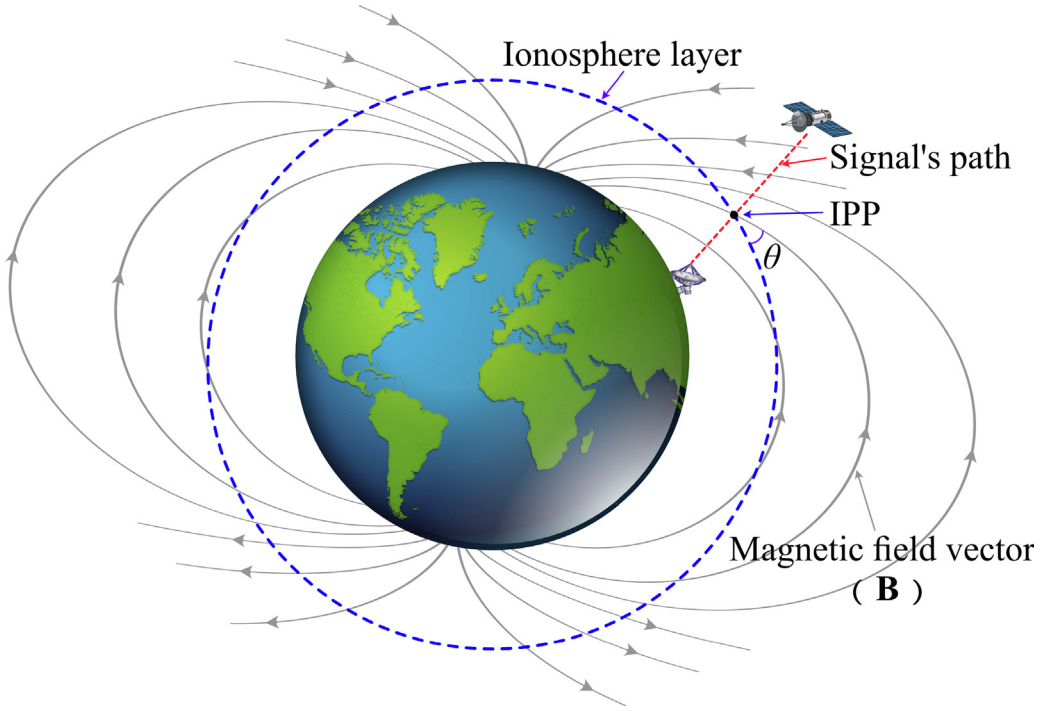

Fig. 2. The ionosphere layer between ground station and spacecraft is simplified as a single layer (blue dashed curve). Passing the signal (red dashed line) between a spacecraft and a ground station through the ionospheric pierce point (IPP), the magnetic field vector $\boldsymbol{B}$ and its angle θ to ionosphere layer at IPP can be acquired by a magnetic field model.

where the TEC value can be solved at certain time epoch t by iterative computations. The residual errors for Eq. (29) are mainly originated from the assumption of single layer ionosphere. However, the errors introduced by this simplification will not exceed 2 mm at the most extreme conditions for GPS dual-frequency (Hoque and Jakowski, 2008). Moreover, if we have a sufficient time for an experiment (e.g. from several days to a month), the average influence of ionospheric shift can be corrected at better than 1 mm level, corresponding to one magnitude improvement at least. This improvement ratio is also valid for other frequencies. For the ACES case, considering the f^{-3} and f^{-4} terms, $\delta f_{ion}/f$ can be enhanced to 8.8×10^{-18}.

Since the tropospheric shift was cancelled out in the three links combination scheme, the error term ϵ in Eq. (10) has no effect for an ideal case. The residual errors of tropospheric shift are only originated from the discrepancy between the downlink path and uplink path, which will be explained in Section 3.3.

3.3. Path discrepancy between downlink and uplink

In previous analysis, it is assumed that the uplink and downlink paths in the three links combination scheme are identical, which is not strictly holding. Because of the Earth's rotation, the uplink and downlink signals paths are different slightly (as depicted in Fig. 3, the downlink paths of f_1 and f_2 cannot be considered as identical), therefore, the classical Doppler shift, tropospheric and ionospheric shift are not cancelled out completely. However, definite corrections for these effects can be adopted, for which the magnitudes of residual errors are estimated in this subsection.

Suppose the path of the ground station P and the spacecraft's orbit are spherical, the orbit radius of the spacecraft is R_s at a certain time point. The elevation angle of the spacecraft from the ground station at the emitting time of uplink is θ_p and the angle between uplink and downlink signals is θ_s. We represent the velocities of ground station as $\boldsymbol{v_p}$ and $\boldsymbol{v_{p'}}$ for P and P', the position vector between the spacecraft and the ground station as $\boldsymbol{r_{sp}}$ and $\boldsymbol{r_{sp'}}$, and the velocity of spacecraft as $\boldsymbol{v_s}$. Furthermore, the centripetal acceleration of P is $\boldsymbol{a_p} = \mathrm{d}\boldsymbol{v_p}/\mathrm{d}t$. $\boldsymbol{N_{sp}} = \boldsymbol{r_{sp}}/r_{sp}, \boldsymbol{N_{sp'}} = \boldsymbol{r_{sp'}}/r_{sp'}$. Suppose the time difference between signal's emitting time and receiving time of ground station is Δt which is a small amount (about $0.1 \sim 0.2$ s for GNSS satellite, $0.003 \sim 0.004$ s for ISS). Thus, we have $\Delta t = 2r_{sp}/c$, and the residual of classical Doppler shift for the three links combination reads:

$$\begin{aligned}\frac{\Delta f'_{dop}}{f_0} &= \frac{1}{2c}\left[\boldsymbol{N_{sp}}\cdot\left(\boldsymbol{v_s}-\boldsymbol{v_p}\right)-\boldsymbol{N_{sp'}}\cdot\left(\boldsymbol{v_s}-\boldsymbol{v_{p'}}\right)\right]\\ &= \frac{1}{2c}\left[\boldsymbol{N_{sp}}\cdot\boldsymbol{v_{sp}}-\left(\boldsymbol{N_{sp}}+\frac{\left(\boldsymbol{v_p}+v_p\cdot\cos\theta_p\cdot\boldsymbol{N_{sp}}\right)\cdot\Delta t}{r_{sp}}\right)\cdot\left(\boldsymbol{v_{sp}}-\boldsymbol{a_p}\cdot\Delta t\right)\right]\\ &= \frac{\boldsymbol{a_p}\cdot\boldsymbol{r_{sp}}}{c^2}-\frac{\boldsymbol{v_{sp}}\cdot\left(\boldsymbol{v_p}+v_p\cdot\cos\theta_p\cdot\boldsymbol{N_{sp}}\right)}{c^2}+\frac{2r_{sp}\cdot\boldsymbol{a_p}\cdot\left(\boldsymbol{v_p}+v_p\cdot\cos\theta_p\cdot\boldsymbol{N_{sp}}\right)}{c^3},\end{aligned} \tag{30}$$

where $\boldsymbol{v_{sp}} = \boldsymbol{v_s} - \boldsymbol{v_p}$. Since $a_p < 3.4 \times 10^{-2}$ m s^{-2} and $v_p < 470$ m s^{-1} (maximum values at the equator), the magnitudes of the three right side terms of Eq. (30) can reach

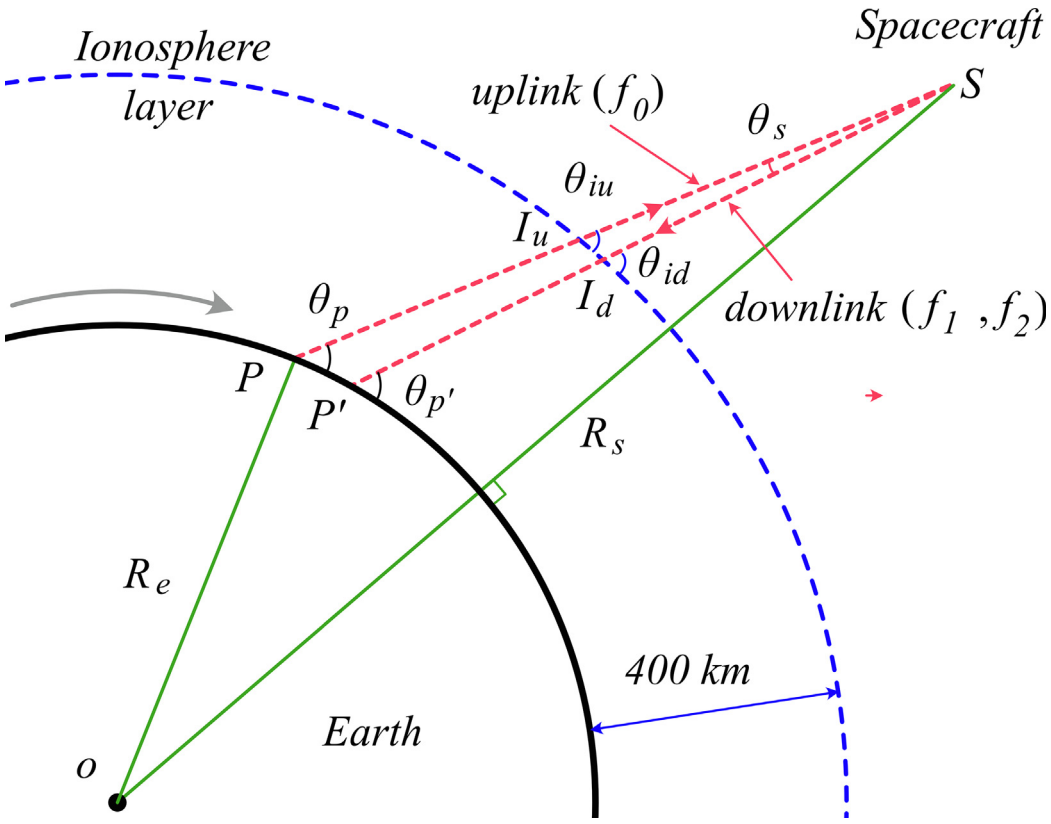

Fig. 3. The ground station is considered as P and P' for the emitting and receiving times of frequency signals. The spacecraft is denoted as S and the ionosphere is simplified as a single layer represented as dashed curve. The uplink path and downlink path are PS and SP', respectively, and the IPP of uplink and downlink are I_u and I_d respectively. The elevation angles of PS and $P'S$ are θ_p and $\theta_{p'}$, respectively. The angle between uplink path and ionosphere layer is θ_{iu}, and the angle between downlink path and ionosphere layer is θ_{id}. R_e is the Earth's radius, and R_s is the orbit radius of spacecraft. The spacecraft's orbit and Earth's surface are simplified as a sphere.

$10^{-12}, 10^{-11}$ and 10^{-17} levels, respectively. Eq. (30) is consistent with the theoretical formula presented by Vessot and Levine (1979). Indeed, Vessot's formula is a special case of this work, in which a dedicated combination of three frequencies was adopted. Vessot and Levine (1979) also neglected the whole c^{-3} term and part of the second term ($v_p \cdot \cos\theta_p \cdot \boldsymbol{N_{sp}}/c^2$ is neglected) in Eq. (30), ignored the c^{-3} term in Eq. (4), because the precision requirement is only 10^{-15} in that paper.

If our precision requirement for Δf_{grav} is higher than 10^{-17}, all these terms need to be considered and calculated. Since the Earth's angular velocity is about 7.292115×10^{-5} rad s^{-1} with the relative uncertainty 1.4×10^{-8} (Groten, 2000), there is the acceleration uncertainty $\delta a_p < 1.5 \times 10^{-9}$ m s^{-2}. Based on the previous estimation, we have $\delta r_{sp} \sim 1$ cm, $\delta v_s \sim 10^{-5}$ m s^{-1}, therefore, the residual error of classical Doppler shift after the path correction is $\delta f'_{dop}/f_0 < 4.4 \times 10^{-19}$.

The Path discrepancy has no effect in TEC determination for Eq. (20) since the paths of f_1 and f_2 can be considered as identical. However, the TEC variation value for Eq. (14), namely the $TEC(t)$ and $\dot{TEC}(t)$ values for uplink are different slightly from downlink, which needs to be considered. We also adopted the IPP simplification here for an easier estimation of the residual of ionospheric shift, where the height of the ionosphere layer is supposed as 400 km above ground for GNSS (Kedar et al., 2003). Then, based on Fig. 3 we have

$$VTEC(t) = \sin\theta_{iu} \cdot TEC_u(t) = \sin\theta_{id} \cdot TEC_d(t), \tag{31}$$

where $VTEC$ represents the vertical total electron content, assuming that the $VTEC$ for uplink IPP and downlink IPP are identical. θ_i is the angle between ionosphere layer and signal's path, the subscript u and d represent uplink and downlink, respectively. It is worth noting that the value $TEC_d(t)$ is known value, which is solved by Eq. (20), then, $TEC_u(t)$ can be obtained based on the angles θ_{iu} and θ_{id}, expressed as:

$$\begin{aligned} \theta_{iu} &= \frac{\pi}{2} - \arccos\frac{\overline{PI_u}^2 + (R_e+400000)^2 - R_g^2}{2\overline{GI_u}(R_e+400000)} \\ \theta_{id} &= \frac{\pi}{2} - \arccos\frac{\overline{P'I_d}^2 + (R_e+400000)^2 - R_g^2}{2\overline{G'I_d}(R_e+400000)}, \end{aligned} \tag{32}$$

where $\overline{PI_u}$ and $\overline{P'I_d}$ can be determined based on the law of cosines:

$$\begin{aligned}\overline{PI_u} &= R_e\cos\theta_p + \sqrt{R_e^2\cos^2\theta_p - R_e^2 + (R_e+400000)^2}\\ \overline{P'I_d} &= R_e\cos\theta_{p'} + \sqrt{R_e^2\cos^2\theta_{p'} - R_e^2 + (R_e+400000)^2}.\end{aligned} \tag{33}$$

where the elevation values θ_p and $\theta_{p'}$ can be calculated in terms of the satellite ephemeris.

Based on Eqs. (31), (33), $TEC_u(t)$ can be obtained, then, as TEC variation $\dot{TEC}_u(t)$ and $\dot{TEC}_d(t)$ are calculated by Eq. (22), the coefficient C_2 in Eq. (14) is extended as:

$$C_2 = b^{-2} - 0.5a^{-2} - 0.5\rho \tag{34}$$

where ρ is the ratio $\dot{TEC}_u(t)/\dot{TEC}_d(t)$.

To estimate the effect magnitude of path discrepancy for ionospheric shift $\Delta f'_{ion}$, we assume the spacecraft is a GNSS satellite (height of about 20 000 km, frequency f_0 of 1.4 GHz, elevation angle of higher than 20°) and the ground station placed at the equator. Then, based on the numerical calculations,$\Delta f'_{ion}/f_0 < 1.4\times10^{-17}$. This path discrepancy residual will rapidly decrease by increasing the signal's frequency. For the ACES case (height of about 400 km, frequency f_0 of 13.5 GHz), the assumed height of ionosphere layer is smaller than that for the GNSS case, because it occupies only a part of ionosphere. But the correction method for ACES is identical except for a different height of ionospheric layer. And the influence of ionosphere related path discrepancy for ISS is obviously smaller than that for GNSS (because of shorter signal's transmitting time and smaller depth of ionosphere). Hence, it is safe to apply the estimation equation of GNSS case to ACES case. The result shows that for ACES case, $\Delta f'_{ion}/f_0$ is decreased to $< 1.8\times10^{-20}$, which is neglectable if the scaling factor C_2/C_1 is not too large (Eq. (37)).

The residual errors $\delta f'_{ion}$ after correction are mainly originated from (1) simplifying the single ionosphere layer, and (2) assuming the identical $VTEC$ at I_u and I_d. In our work, further numerical estimations of these two influences are not presented. But notice that the single ionosphere layer simplification is widely used in GNSS positioning and proved to be effective; and the second group errors are random errors that can be reduced followed by the average of an adequate period of observations. Furthermore, for most cases the $\Delta f'_{ion}$ is smaller than its max value, since it will rapidly decrease by increasing elevation angle θ_p (at least two magnitudes smaller than its max value when $\theta_p = 90°$). Thus, it is reasonable to assume that $\delta f'_{ion}$ is at least one magnitude smaller than $\Delta f'_{ion}$.

The estimation of the tropospheric shift residual is much more straightforward, since we can adopt certain tropospheric propagation delay models extensively used in GNSS positioning Saastamoinen model (Saastamoinen, 1972), Black model (Black, 1978) to estimate the integral amount $\int_L N(t)\mathrm{d}s$ in Eq. (11). Specifically, the tropospheric delay can be divided into the wet and dry components, then their zenith tropospheric delay (ZTD) are estimated first. Thus, the tropospheric delay of a slant direction can be calculated by applying mapping functions to each component (Leick et al., 2015). Considering the tropospheric influence as $I_{trop}(t,\theta) = \int_L N(t)\mathrm{d}s$, then:

$$\begin{aligned}I_{trop}(t,\theta) &= \int_L N_{dry}(t)\mathrm{d}s + \int_L N_{wet}(t)\mathrm{d}s\\ &= \int_{zenith} N_{dry}(t)\mathrm{d}s\cdot M_{dry}(t,\theta) + \int_{zenith} N_{wet}(t)\mathrm{d}s\cdot M_{wet}(t,\theta),\end{aligned} \tag{35}$$

where θ denotes elevation angle, M_{dry} and M_{wet} represent mapping functions of dry and wet components of zenith delay. In Eq. (35), the zenith delay $\int_{zenith} N_{dry}(t)\mathrm{d}s$ and $\int_{zenith} N_{wet}(t)\mathrm{d}s$ can be estimated through meteorological elements (temperature, pressure and humidity) at the ground station. Such elements can be obtained by direct measurement or by an atmosphere model such as Earth Global Reference Atmospheric Model (Leslie and Justus, 2011). There are various slightly different expressions for mapping functions, among which the GPT2 model (Lagler et al., 2013) is normally preferred, and consequently we used this model here. The values of $M_{dry}(t,\theta)$ and $M_{wet}(t,\theta)$ can be obtained directly by the model, for which the details can be referred to (Boehm et al., 2006; Lagler et al., 2013). Thus, the tropospheric influence $I_{trop}(t,\theta) = \int_L N(t)\mathrm{d}s$ can be calculated, while estimating its time differential $\dot{I}_{trop}(t,\theta)$ by continuous observation similar to Eq. (22).

Considering the path discrepancy and Eqs. (11), (12) and (35), the residual of tropospheric shift for the three links combination scheme is obtained:

$$\frac{\Delta f'_{trop}}{f_0} = \frac{1}{2c}\left(\dot{I}_{trop}(t,\theta_{p'}) - \dot{I}_{trop}(t,\theta_p)\right), \tag{36}$$

where the residual amount is based on the difference between θ_p and $\theta_{p'}$, which normally increases by decreasing the elevation angle. Suppose the ground station is located at the Earth's equator and the spacecraft is a GNSS satellite, then under the standard atmosphere model we have $\Delta f'_{trop}/f_0 < 2.3\times10^{-16}$ if the satellite's elevation angle is higher than 20°. Since the tropospheric delay model has a precision better than 95%, the residual errors of path discrepancy for tropospheric shift after correction is $\delta f'_{trop}/f_0 < 1.1\times10^{-17}$. Correspondingly, it is estimated that the residual errors for ACES are smaller than 5.3×10^{-18}.

In real world the error of a single observation sample might be larger than the estimation above because of various factors (model resolution, smoothness et al.). But for continuous observations lasting for several days or a month, the average result is likely to be close to our prediction. Ultimately, it is worth noting that for most real cases when the ground station is not located at the Earth's equator, the path discrepancy will have smaller influences than

the numerical results (classical Doppler, ionospheric and tropospheric shift) provided in this subsection.

3.4. Other effect

All the noises, known and unknown minor error effects during the experiment are included in the last term Δf_{oth} in Eq. (2). Referring to existing spacecraft-based applications and experiments, they most can be corrected or compensated by some techniques (Litvinov et al., 2018; Delva et al., 2018; Savalle et al., 2019). For instance, the on-board atomic clock might be affected by temperature and magnetic field, which could be corrected by a magnetic field model and a temperature field model, or more precisely by the on-board magnetometer and thermometer. The residual errors can be considered as part of clock noises reflecting the clock stability. The phase wind-up and phase center motion of the on-board antennas can be calculated from orbital and housekeeping data (Moyer, 2003). The instrumental delays can be pre-calibrated to reduce its influence to frequency observations. Moreover, they also have slight effects in dual-frequency TEC determination process when they are pre-calibrated and compensated consequently in Eq. (21). Furthermore, if some error sources are proportional to signal's frequency, they are also cancelled out in the three frequencies combination scheme described in Section 2.2.

Here, a full list of error sources is not presented, however, their influence is safely assumed to be < 5 cm in frequency shift detection after adequate corrections. The reason is that the precise point positioning (PPP) technique can reach 1 cm in height determination (Kaplan and Hegarty, 2017) adopting similar error correction methods. Indeed, the main error sources in δf_{oth} would be clock noise, since for a precision of 1 cm in gravitational redshift detection, the fractional frequency stability of atomic clock needs to reach 10^{-18}. Currently, this is only achievable in ground laboratories; and the stability of on-board clock is assumed to be 10^{-17} in our test. Therefore, the magnitude of δf_{oth} is estimated to be 1.2×10^{-17}.

The stability of ground clock is usually 1̨2 magnitudes better than that of the on-board clock, hence its direct influence for δf_{oth} can be neglected. However, its instability will affect the precision of the measured time interval Δt in Eq. (21), consequently affect the precision of TEC determination. For instance, suppose that the ground clock instability is about $1 \times 10^{-16}/\sqrt{\tau}$, where τ is time in second (the precision level has been exceeded by Oelker et al. (2019)). Then the time uncertainty δt for Eq. (21) is only 0.1 fs for GNSS case which is neglectable. In fact, the main influence of δt is the digital noise within the receiver, which is assumed to be 3 ps for each measurement. The instrumental delay on spacecraft may also cause a small asynchrony of the emitting time of f_1 and f_2, but this difference can be pre-calibrated and the residual is neglected because it is much smaller than the digital noise within the receiver.

Then we have $\delta t = 3\sqrt{2}$ ps, which will cause 1.2×10^{14} el·m^{-2} in TEC uncertainty and thus 1.4×10^{-14} in $\Delta f_{ion}/f$ uncertainty (denoted as $\delta f''_{ion}/f$). However, the estimations above are oriented by one single measurement. Based on the statistical characteristics of receiver's noise, the uncertainty $\delta f''_{ion}/f$ will be greatly reduced followed by adequate time of observations. Suppose the sample rate is 1 observations per second, and 24 h' observation data are available (It requires that the experiment time be more than one day, because the spacecraft and ground station are not always inter-visible), then $\delta f''_{ion}/f$ is about 4.7×10^{-17} for GNSS case and 6.9×10^{-19} for ACES case.

3.5. Accuracy of gravitational redshift test

In previous subsections, we analyzed the magnitudes of all the error sources affecting the satellite EEP test experiment. Noted that some of them are analyzed under the one-link case and should be extended to three-link case based on Eq. (12). Then, according to Eqs. (2) and (23), the total uncertainty of frequency shift δf_{all} can be estimated in terms of the law of error propagation:

$$\delta f_{all} = \left[\delta f_{rel}^2 + \left(\frac{C_2\delta f_{ion}}{C_1}\right)^2 + \left(\frac{\delta f'_{dop}}{C_1}\right)^2 + \left(\frac{C_2\delta f'_{ion}}{C_1}\right)^2 + \left(\frac{\delta f'_{trop}}{C_1}\right)^2 + \left(\frac{C_2\delta f''_{ion}}{C_1}\right)^2 + \left(\frac{\delta f_{oth}}{C_1}\right)^2 \cdot \left(\frac{1}{b^2} + \frac{1}{(2a)^2} + \frac{1}{2^2}\right)\right]^{0.5}. \quad (37)$$

where a and b are defined in Section 2.2. The classical Doppler shift term δf_{dop} and tropospheric shift term δf_{trop} are not involved in Eq. (37) since they are cancelled out in the three-link combination scheme (their path discrepancy effect is included). The uncertainty of observed value f_{out} is also not considered because it is reflected in the δf_{oth} term. After obtaining the δf_{all} value by Eq. (37), the precision of EEP test can be estimated based on Eq. (24). The uncertainty of $\delta\alpha$ achieved based on the three link method as along with the magnitudes of various error sources are listed in Table 1. The precision of on-board clocks in Table 1 are assumed as 10^{-17}/day. We estimated three different cases: (1) A GPS satellite using 1.227 GHz and 1.575 GHz as downlink frequencies, where the uplink frequency is assumed as 1.4 GHz; (2) The ACES project on ISS employing 2.248 GHz and 14.7 GHz as downlink frequencies, and 13.475 GHz as the uplink frequency; (3) An assumed satellite using 8 GHz and 12 GHz as downlink frequencies, and 10 GHz as the uplink frequency, for which the orbit height are similar to a GPS satellite (about 20 000 km).

3.6. Accuracy improvements

In previous subsection we analyzed three cases adopting different frequency values, which possess different satellite orbits. It is observed that the Assumed Case greatly improves the overall accuracy for EEP test, from 10^{-6} level to 10^{-7} level, compared to the GNSS or ISS cases. There

Table 1
The theoretical uncertainties of various error sources and the ultimate precision of EEP test experiment, based on three-link combination. All the three cases (GPS, ACES and Assumed) are estimated under the assumption that the precision of on-board clocks reach 10^{-17}/day level. The experiment period is from several days to a month. The magnitudes provided here are residuals after different corrections described in Section 3, and δf_{all} are estimated based on Eq. (37).

Uncertainty of frequency shift components		Symbol	Residual magnitudes for different cases		
			GPS	ACES	Assumed
Classical Doppler shift		$\delta f_{dop}/f_0$	Neglectable	Neglectable	Neglectable
Relativistic shift		$\delta f_{rel}/f_0$	$\sim 2.9\times10^{-18}$	$\sim 5.0\times10^{-17}$	$\sim 2.9\times10^{-18}$
Ionospheric shift		$\delta f_{ion}/f_0$	$\sim 7.9\times10^{-15}$	$\sim 8.8\times10^{-18}$	$\sim 2.2\times10^{-17}$
Tropospheric shift		$\delta f_{trop}/f_0$	Neglectable	Neglectable	Neglectable
Path discrepancy	Doppler	$\delta f'_{dop}/f_0$	$< 4.4\times10^{-19}$	$< 6.2\times10^{-19}$	$< 4.4\times10^{-19}$
	Ionosphere	$\delta f'_{ion}/f_0$	$< 1.4\times10^{-18}$	$< 1.8\times10^{-21}$	$< 2.7\times10^{-20}$
	Troposphere	$\delta f'_{trop}/f_0$	$< 1.1\times10^{-17}$	$< 5.3\times10^{-18}$	$< 1.1\times10^{-17}$
Iono. shift uncertainty caused by δt		$\delta f''_{ion}/f_0$	$\sim 4.7\times10^{-17}$	$\sim 6.9\times10^{-19}$	$\sim 2.7\times10^{-17}$
Clock errors and other minor effects		$\delta f_{oth}/f_0$	$\sim 1.2\times10^{-17}$	$\sim 1.2\times10^{-17}$	$\sim 1.2\times10^{-17}$
Total uncertainty of frequency shift		$\delta f_{all}/f_0$	$\sim 3.5\times10^{-15}$	$\sim 1.1\times10^{-16}$	$\sim 3.7\times10^{-17}$
Uncertainty of EEP test		$\delta\alpha$	$\sim 6.5\times10^{-6}$	$\sim 2.2\times10^{-6}$	$\sim 7.3\times10^{-8}$

are some patterns for improving the EEP test accuracy, moreover, this Assumed Case does not include the best achievable accuracy (In fact, the orbit and frequencies are not very special). In this subsection, we will discuss relationship between the experiment setup for that EEP test accuracy.

The first method to enhance accuracy is to increase the frequency values of the links making the TEC determination more accurate, hence, the ionospheric shift residual $\delta f_{ion}/f_0$ is Reduced. For example, the ionospheric shift residual of ACES case is much smaller than GNSS case as shown in Table 1. Nevertheless, this improvement has some costs on clock accuracy influence $\delta f''_{ion}/f_0$ which will be discussed later; higher frequency values does not definitely lead to the higher EEP test accuracy.

The second method to enhance accuracy is to select a frequency combination with small C_2/C_1 value reducing the residual of ionospheric shift as well. This is a method typically adopted in the GP-A experiment, which in fact makes $C_2/C_1 = 0$. On the contrary, high C_2/C_1 value will largely extend the effects of ionosphere. For instance, the C_2/C_1 of ACES case reaches 11.2 whereas the GNSS case is only 0.4. Thus, although the ACES case benefits from higher frequency values, its overall accuracy has no much enhancement compared to GNSS case. They both are limited in 10^{-6} level as shown in Table 1. As for the Assumed Case with frequencies selected casually (8Ghz, 10Ghz and 12Ghz), its $C_2/C_1 = 0.83$ has still much room for improvement in case its frequencies are chosen more specifically.

The third method to improve accuracy is to increase the time difference Δt between the received time of the two downlink signals f_1 and f_2, hence, for a given δt the effect of receiver noise in $\delta f''_{ion}/f_0$ decreases. This can be obtained by increasing the frequency difference between f_1 and f_2, or reducing the overall frequency values. For instance, the GNSS adopts very low frequencies ($1\tilde{2}$ GHz for three links) and its $\delta f''_{ion}/f_0$ is smallest. ISS has very large (2.248 GHz and 14.7 GHz) frequency difference of the two downlinks, hence, its $\delta f''_{ion}/f_0$ is smaller than the Assumed Case with downlink frequencies of 8 GHz and 12 GHz. However, it is obvious that the third method is constrained by the second one and contradicts the first method. The best performance is to make a balanced frequency selection presenting $\delta f_{ion}/f_0 \approx \delta f''_{ion}/f_0$ while C_2/C_1 is as low as possible.

The fourth influence factor for the EEP test is the spacecraft's height. In general, higher orbit will result in the larger gravitational potential difference ΔU in Eq. (24) and accordingly a better EEP test uncertainty $\delta\alpha$. It also reduces the uncertainty of Shapiro effect and thus the $\delta f_{rel}/f_0$ value. Nevertheless, higher orbit will increase the signals' transmitting time resulting in the increased path discrepancy (Fig. 3). Consequently, its residual is increased (in Table 1, the path discrepancy residual of GNSS and Assumed Case are higher than that of ACES case). Furthermore, we estimated the path discrepancy influence of ionosphere and troposphere in Section 3.3 assuming that the VTEC and ZTD of uplink and downlink are identical. By the too large path discrepancy of uplink and downlink, this assumption might be weak and cause more residual errors. Thus, the orbit height of spacecraft should also be selected in balance.

Ultimately, it should be noted that we can not present a "best" frequencies and orbit height values here, since it largely based on the precision of hardware as along with our knowledge to the atmosphere. In addition, if our techniques are improved to the extent where the influences of most error sources is decreased to 10^{-18} level or even better, the J_2-terms of Shapiro effect must be considered, which is left for future investigation.

4. Conclusion

In this paper, we proposed a three-link combination technique based on frequency signals links between a ground station and a spacecraft to test gravitational redshift effect. The test can be performed according to our setup by any spacecraft (low-orbit type, GNSS type, and

geostationary type) with frequency signal receiver and emitter. Therefore, many spacecrafts, such as ISS and CSS, have potential to carry out the gravitational redshift experiment. Furthermore, a GNSS satellite (with at least two frequency signal emitters currently) can meet the experiment requirements by arming it with a frequency signal receiver. Besides, the precision of this method is also satisfying, about $10^{-6} \sim 10^{-8}$ for $\delta\alpha$ determination given different conditions, which is at least one magnitude better compared to the current EEP test. It can be predicted that the gravitational redshift research and its application will be promoted greatly since the experiment is simple.

Noted that in this paper we aim to measure the redshift between ground station and spacecraft, thus the experiment procedure is different from the EEP test experiments on eccentric Galileo satellites which measured redshift variations (Delva et al., 2018; Herrmann et al., 2018). Specifically, before the launch of the spacecraft, the on-board clock should be calibrated with the clock of the target ground station; in addition, various hardware delays and frequency offsets should also be calibrated. After the launch of the spacecraft, the EEP test experiment should be immediately started, and the on-board clock cannot be steered during the experiment. Although the experiment procedure has more restrictions compared to the EEP test on eccentric Galileo satellites, it has the merits. For example, the experiment we proposed can be conducted at a spacecraft regardless of eccentric orbit or circular orbit; and the precision of α coefficient is higher than experiments that measure redshift variations.

The three-link combination method also can be utilized in gravitational potential determination. If α is given (currently it is safe to assume that $\alpha = 0$) while the ΔU is unknown, the gravitational potential difference between a ground station and a spacecraft can be obtained after the Δf_{rel} is derived based on Eq. (23). Moreover, the precision of the determined gravitational potential is related to $\delta f_{fall}/f_0$ value. Based on the experiment setup in Section 3.5, the precision of ΔU is about 3.5×10^2 m^2s^{-2} for GNSS case, 11 m^2s^{-2} for ACES case and 3.7 m^2s^{-2} for Assumed Case, equivalent to about 35 m, 1.1 m and 0.37 m in height, respectively. The relativistic technique of gravitational potential determination is also a very promising subject in geodesy. Once the precision can reach 1 cm level (corresponding to $f_{all}/f_0 \sim 10^{-18}$), the three-link combination technique will be appropriate for practical application in gravitational potential determination.

In addition to the patterns we discussed in Section 3.6, there are some other possible techniques to enhance the precision of satellite based EEP test experiment (or gravitational potential determination). In fact, it requires an upgrade of the three-link combination method. For instance, if we add another downlink signal (three downlinks in total), the TEC can be derived more precisely and the ionosphere-related residual errors may be reduced. For similar purpose, three downlink frequencies have been applied in modern GNSS satellite (Kaplan and Hegarty, 2017). Moreover, if we add another uplink signal (two uplinks and two downlinks are adopted in the planned CSS mission), the residual errors of path discrepancy can be reduced, and the reliability of EEP test can be enhanced by using two different base frequencies. Another important influence factor is the clock precision in the experiment. In our error estimation, we assumed that the clock stability can reach 10^{-17}/day, which is only achievable in ground laboratories. By reducing the stability of on-board atomic clocks one magnitude (10^{-16}/day), the $\delta\alpha$ of the GPS, ACES and Assumed cases will increase to $6.6 \times 10^{-6}, 4.5 \times 10^{-6}$ and 3.1×10^{-7}, respectively. However, if the on-board atomic clocks can reach 10^{-18}/day (now achievable in ground laboratories), $\delta\alpha$ of the three cases all have no obvious improvements. These estimations confirm that the main error sources are not from clock errors if the clock stability is better than 10^{-17}/day. Finally, it should be noted that the numerical error analysis results are based on a relatively short period of experiment (several days to a month). If long-term observation data are available (the results of EEP test on two Galileo satellites (Delva et al., 2018; Herrmann et al., 2018) are based on nearly 3 years of observation data), the precision of $\delta\alpha$ would be better than our error analysis results after comprehensive data processing.

Declaration of Competing Interest

The authors declare that they have no competing financial interests or personal relationships that could have appeared to influence the work reported in this paper.

Acknowledgements

This study is supported by National Natural Science Foundation of China (NSFC) (Grant Nos. 42030105, 41721003, 41631072, 41874023, 41804012), Space Station Project (2020)228, and Natural Science Foundation of Hubei Province (Grant No. 2019CFB611).

References

Altschul, B., Bailey, Q.G., Blanchet, L., Bongs, K., Bouyer, P., Cacciapuoti, L., Capozziello, S., Gaaloul, N., Giulini, D., Hartwig, J., Iess, L., Jetzer, P., Landragin, A., Rasel, E., Reynaud, S., Schiller, S., Schubert, C., Sorrentino, F., Sterr, U., Tasson, J.D., Tino, G.M., Tuckey, P., Wolf, P., 2015. Quantum tests of the einstein equivalence principle with the STE–QUEST space mission. Adv. Space Res. 55 (1), 501–524.

Bjerhammar, A., 1985. On a relativistic geodesy. Bull. Am. Assoc. Hist. Nurs. 59 (3), 207–220.

Black, H.D., 1978. An easily implemented algorithm for the tropospheric range correction. J. Geophys. Res. 83 (B4), 1825–1828.

Blanchet, L., Salomon, C., Teyssandier, P., Wolf, P., 2001. Relativistic theory for time and frequency transfer to order c-3. Astron. Astrophys. 370 (1), 320–329.

Boehm, J., Werl, B., Schuh, H., 2006. Troposphere mapping functions for GPS and very long baseline interferometry from european centre for

medium-range weather forecasts operational analysis data. J. Geophys. Res. 111 (B2).
Brunner, F.K., Gu, M., 1991. An improved model for the dual frequency ionospheric correction of GPS observations. Manuscripta Geodaetica 16 (3), 205–214.
Cacciapuoti, L., Salomon, C., 2011. Atomic clock ensemble in space (ACES). European Space Agency, (Special Publication) ESA SP 327 (385), 295–297.
Corstanje, A., Bonardi, A., Buitink, S., Falcke, H., Hörandel, J.R., Mitra, P., Mulrey, K., Nelles, A., Rachen, J.P., Rossetto, L., Schellart, P., Scholten, O., ter Veen, S., Thoudam, S., Trinh, G., Winchen, T., 2017. The effect of the atmospheric refractive index on the radio signal of extensive air showers. Astropart. Phys. 89, 23–29.
Davies, K., Watts, J.M., Zacharisen, D.H., 1962. A study of F 2 -layer effects as observed with a doppler technique. J. Geophys. Res. 67 (2), 601–609.
Delva, P., Denker, H., Lion, G., 2019. Chronometric geodesy: Methods and applications. In: Puetzfeld, D., Lämmerzahl, C. (Eds.), Relativistic Geodesy: Foundations and Applications. Springer International Publishing, Cham, pp. 25–85.
Delva, P., Hees, A., Bertone, S., Richard, E., Wolf, P., 2015. Test of the gravitational redshift with stable clocks in eccentric orbits: application to galileo satellites 5 and 6. Classical Quantum Gravity 32 (23), 232003.
Delva, P., Puchades, N., Schönemann, E., Dilssner, F., Courde, C., Bertone, S., Gonzalez, F., Hees, A., Le Poncin-Lafitte, C., Meynadier, F., Prieto-Cerdeira, R., Sohet, B., Ventura-Traveset, J., Wolf, P., 2018. Gravitational redshift test using eccentric galileo satellites. Phys. Rev. Lett. 121 (23), 231101.
Einstein, A., 1915. Die feldgleichungen der gravitation. Sitzungsberichte der Königlich Preußischen Akademie der Wissenschaften (Berlin).
Folkner, W.M., Williams, J.G., Boggs, D.H., Park, R.S., Kuchynka, P., 2014. The planetary and lunar ephemerides DE430 and DE431. Interplanetary Network Progress Report 196 (1).
Griffiths, J., Ray, J.R., 2009. On the precision and accuracy of IGS orbits. J. Geodesy 83 (3), 277–287.
Groten, E., 2000. Parameters of common relevance of astronomy, geodesy, and geodynamics. J. Geodesy 74 (1), 134–140.
Grotti, J., Koller, S., Vogt, S., Häfner, S., Sterr, U., Lisdat, C., Denker, H., Voigt, C., Timmen, L., Rolland, A., Baynes, F.N., Margolis, H.S., Zampaolo, M., Thoumany, P., Pizzocaro, M., Rauf, B., Bregolin, F., Tampellini, A., Barbieri, P., Zucco, M., Costanzo, G.A., Clivati, C., Levi, F., Calonico, D., 2018. Geodesy and metrology with a transportable optical clock. Nat. Phys. 14 (5), 437–441.
Hernández-Pajares, M., Juan, J.M., Sanz, J., 1999. New approaches in global ionospheric determination using ground GPS data. J. Atmos. Sol. Terr. Phys. 61 (16), 1237–1247.
Herrmann, S., Finke, F., Lülf, M., Kichakova, O., Puetzfeld, D., Knickmann, D., List, M., Rievers, B., Giorgi, G., Günther, C., Dittus, H., Prieto-Cerdeira, R., Dilssner, F., Gonzalez, F., Schönemann, E., Ventura-Traveset, J., Lämmerzahl, C., 2018. Test of the gravitational redshift with galileo satellites in an eccentric orbit. Phys. Rev. Lett. 121 (23), 231102.
Hoque, M.M., Jakowski, N., 2007. Higher order ionospheric effects in precise GNSS positioning. J. Geodesy 81 (4), 259–268.
Hoque, M.M., Jakowski, N., 2008. Estimate of higher order ionospheric errors in GNSS positioning. Radio Sci. 43 (5).
Kang, Z., Tapley, B., Bettadpur, S., Ries, J., Nagel, P., Pastor, R., 2006. Precise orbit determination for the GRACE mission using only GPS data. J. Geodesy 80 (6), 322–331.
Kaplan, E., Hegarty, C.J., 2017. Understanding GPS/GNSS: Principles and Applications, Third Edition, 3rd ed. Artech House, Inc., USA.
Kedar, S., Hajj, G.A., Wilson, B.D., Heflin, M.B., 2003. The effect of the second order GPS ionospheric correction on receiver positions: Second Order IONOSPHERE GPS CORRECTION. Geophys. Res. Lett. 30 (16), 1009.
Kleppner, D., Vessot, R.F.C., Ramsey, N.F., 1970. An orbiting clock experiment to determine the gravitational red shift. Astrophys. Space Sci. 6 (1), 13–32.
Kopeikin, S.M., Kanushin, V.F., Karpik, A.P., Tolstikov, A.S., Gienko, E.G., Goldobin, D.N., Kosarev, N.S., Ganagina, I.G., Mazurova, E. M., Karaush, A.A., Hanikova, E.A., 2016. Chronometric measurement of orthometric height differences by means of atomic clocks. Gravitation Cosmol. 22 (3), 234–244.
Kovalev, Y.Y., Kardashev, N.S., Kellermann, K.I., Edwards, P.G., 2014. The RadioAstron space VLBI project. In: 2014 XXXIth URSI General Assembly and Scientific Symposium (URSI GASS), p. 1.
Lagler, K., Schindelegger, M., Böhm, J., Krásná, H., Nilsson, T., 2013. GPT2: Empirical slant delay model for radio space geodetic techniques. Geophys. Res. Lett. 40 (6), 1069–1073.
Leick, A., Rapoport, L., Tatarnikov, D., 2015. Troposphere and ionosphere. In: GPS Satellite Surveying. John Wiley & Sons, Inc., Hoboken, NJ, USA, pp. 475–511.
Leslie, F.W., Justus, C.G., 2011. The NASA Marshall Space Flight Center Earth Global Reference Atmospheric Model-2010 Version. Technical Report.
Linet, B., Teyssandier, P., 2002. Time transfer and frequency shift to the order 1/c4 in the field of an axisymmetric rotating body. Phys. Rev. D Part. Fields 66 (2), 024045.
Lion, G., Panet, I., Wolf, P., Guerlin, C., Bize, S., Delva, P., 2017. Determination of a high spatial resolution geopotential model using atomic clock comparisons. J. Geodesy 91 (6), 597–611.
Litvinov, D.A., Rudenko, V.N., Alakoz, A.V., Bach, U., Bartel, N., Belonenko, A.V., Belousov, K.G., Bietenholz, M., Biriukov, A.V., Carman, R., Cimó, G., Courde, C., Dirkx, D., Duev, D.A., Filetkin, A.I., Granato, G., Gurvits, L.I., Gusev, A.V., Haas, R., Herold, G., Kahlon, A., Kanevsky, B.Z., Kauts, V.L., Kopelyansky, G.D., Kovalenko, A.V., Kronschnabl, G., Kulagin, V.V., Kutkin, A.M., Lindqvist, M., Lovell, J.E.J., Mariey, H., McCallum, J., Molera Calvés, G., Moore, C., Moore, K., Neidhardt, A., Plötz, C., Pogrebenko, S.V., Pollard, A., Porayko, N.K., Quick, J., Smirnov, A.I., Sokolovsky, K.V., Stepanyants, V.A., Torre, J.-M., de Vicente, P., Yang, J., Zakhvatkin, M.V., 2018. Probing the gravitational redshift with an earth-orbiting satellite. Phys. Lett. A 382 (33), 2192–2198.
Meynadier, F., Delva, P., le Poncin-Lafitte, C., Guerlin, C., Wolf, P., 2018. Atomic clock ensemble in space (ACES) data analysis. Classical Quantum Gravity 35 (3), 035018.
Moyer, T.D., 2003. Formulation for Observed and Computed Values of Deep Space Network Data Types for Navigation, 1st ed. Wiley-Interscience.
Nakamura, T., Davila-Rodriguez, J., Leopardi, H., Sherman, J.A., Fortier, T.M., Xie, X., Campbell, J.C., McGrew, W.F., Zhang, X., Hassan, Y.S., Nicolodi, D., Beloy, K., Ludlow, A.D., Diddams, S.A., Quinlan, F., 2020. Coherent optical clock down-conversion for microwave frequencies with 10^{-18} instability. Science 368 (6493), 889–892.
Namazov, S.A., Novikov, V.D., Khmel'nitskii, I.A., 1975. Doppler frequency shift during ionospheric propagation of decameter radio waves (review). Radiophys. Quantum Electron. 18 (4), 345–364.
Nunes, N.V., Bartel, N., Bietenholz, M.F., Zakhvatkin, M.V., Litvinov, D.A., Rudenko, V.N., Gurvits, L.I., Granato, G., Dirkx, D., 2020. The gravitational redshift monitored with RadioAstron from near earth up to 350,000 km. Adv. Space Res. 65 (2), 790–797.
Oelker, E., Hutson, R.B., Kennedy, C.J., Sonderhouse, L., Bothwell, T., Goban, A., Kedar, D., Sanner, C., Robinson, J.M., Marti, G.E., Matei, D.G., Legero, T., Giunta, M., Holzwarth, R., Riehle, F., Sterr, U., Ye, J., 2019. Demonstration of $4.8 times 10^{-17}$ stability at 1 s for two independent optical clocks. Nat. Photonics 13 (10), 714–719.
Pavlis, N.K., Holmes, S.A., Kenyon, S.C., et al., 2012. The development and evaluation of the earth gravitational model 2008 (EGM2008). J. Geophys. Res.: Solid Earth 117 (B4), B04406.

Petrie, E.J., Hernández-Pajares, M., Spalla, P., Moore, P., King, M.A., 2011. A review of higher order ionospheric refraction effects on dual frequency GPS. Surv. Geophys. 32 (3), 197–253.

Pi, X., Mannucci, A.J., Lindqwister, U.J., Ho, C.M., 1997. Monitoring of global ionospheric irregularities using the worldwide GPS network. Geophys. Res. Lett. 24 (18), 2283–2286.

Pound, R.V., Rebka, G.A., 1960. Variation with temperature of the energy of recoil-free gamma rays from solids. Phys. Rev. Lett. 4 (6), 274–275.

Rüeger, J.M., 2002. Refractive index formulae for radio waves. In FIG XXII International Congress, Washington, DC, USA, 19-26 April 2002.

Saastamoinen, J., 1972. Atmospheric correction for the troposphere and stratosphere in radio ranging satellites: Henriksen/The use of artificial satellites for geodesy. In: Henriksen, S.W., Mancini, A., Chovitz, B.H. (Eds.), The Use of Artificial Satellites for Geodesy. American Geophysical Union volume 70 of Geophysical Monograph Series, Washington, D.C., pp. 247–251.

Sánchez, L., Sideris, M.G., 2017. Vertical datum unification for the international height reference system (IHRS). Geophys. J. Int. 209 (2), 570–586.

Savalle, E., Guerlin, C., Delva, P., Meynadier, F., le Poncin-Lafitte, C., Wolf, P., 2019. Gravitational redshift test with the future ACES mission. Classical Quantum Gravity 36 (24), 245004.

Shen, Z., Shen, W.-B., Peng, Z., Liu, T., Zhang, S., Chao, D., 2019. Formulation of determining the gravity potential difference using ultra-high precise clocks via optical fiber frequency transfer technique. J. Earth Sci. 30 (2), 422–428.

Shen, Z., Shen, W.-B., Zhang, S., 2016. Formulation of geopotential difference determination using optical-atomic clocks onboard satellites and on ground based on doppler cancellation system. Geophys. J. Int. 206 (2), 1162–1168.

Shen, Z., Shen, W.-B., Zhang, S., 2017. Determination of gravitational potential at ground using optical-atomic clocks on board satellites and on ground stations and relevant simulation experiments. Surv. Geophys. 38 (4), 757–780.

Takamoto, M., Ushijima, I., Ohmae, N., Yahagi, T., Kokado, K., Shinkai, H., Katori, H., 2020. Test of general relativity by a pair of transportable optical lattice clocks. Nat. Photonics 14 (7), 411–415.

Takano, T., Takamoto, M., Ushijima, I., Ohmae, N., Akatsuka, T., Yamaguchi, A., Kuroishi, Y., Munekane, H., Miyahara, B., Katori, H., 2016. Geopotential measurements with synchronously linked optical lattice clocks. Nat. Photonics 10 (10), 662.

Thébault, E., Finlay, C.C., Beggan, C.D., Alken, P., Aubert, J., Barrois, O., Bertrand, F., Bondar, T., Boness, A., Brocco, L., Canet, E., Chambodut, A., Chulliat, A., Coïsson, P., Civet, F., Du, A., Fournier, A., Fratter, I., Gillet, N., Hamilton, B., Hamoudi, M., Hulot, G., Jager, T., Korte, M., Kuang, W., Lalanne, X., Langlais, B., Léger, J.-M., Lesur, V., Lowes, F.J., Macmillan, S., Mandea, M., Manoj, C., Maus, S., Olsen, N., Petrov, V., Ridley, V., Rother, M., Sabaka, T.J., Saturnino, D., Schachtschneider, R., Sirol, O., Tangborn, A., Thomson, A., Tøffner-Clausen, L., Vigneron, P., Wardinski, I., Zvereva, T., 2015. International geomagnetic reference field: the 12th generation. Earth Planets Space 67 (1), 79.

Van Camp, M., Vauterin, P., 2005. Tsoft: graphical and interactive software for the analysis of time series and earth tides. Comput. Geosci. 31 (5), 631–640.

Vessot, R.F.C., Levine, M.W., 1979. A test of the equivalence principle using a space-borne clock. Gen. Relat. Grav. 10 (3), 181–204.

Vessot, R.F.C., Levine, M.W., Mattison, E.M., Blomberg, E.L., Hoffman, T.E., Nystrom, G.U., Farrel, B.F., Decher, R., Eby, P.B., Baugher, C. R., Watts, J.W., Teuber, D.L., Wills, F.D., 1980. Test of relativistic gravitation with a space-borne hydrogen maser. Phys. Rev. Lett. 45 (26), 2081–2084.

Wang, L., Xu, B., Fu, W., Chen, R., Li, T., Han, Y., Zhou, H., 2020. Centimeter-level precise orbit determination for the Luojia-1A satellite using BeiDou observations. Remote Sensing 12 (12), 2063.

Wikipedia contributors, 2021. STE-QUEST — Wikipedia, the free encyclopedia. https://en.wikipedia.org/w/index.php?title=STE-QUEST&oldid=1004195585. Accessed: 2021-4-25.

Will, C.M., 2014. The confrontation between general relativity and experiment. Living Rev. Relativ. 17 (1), 4.

Wolf, P., Petit, G., 1995. Relativistic theory for clock syntonization and the realization of geocentric coordinate times. Astron. Astrophys. 304 (2), 653–661.